LETTER Communicated by Bard Ermentrout

The Influence of Limit Cycle Topology on the Phase Resetting Curve

Sorinel A. Oprisan
soprisan@uno.edu
Carmen C. Canavier
ccanavie@uno.edu
Department of Psychology, University of New Orleans, New Orleans, LA 70148, U.S.A.

Understanding the phenomenology of phase resetting is an essential step toward developing a formalism for the analysis of circuits composed of bursting neurons that receive multiple, and sometimes overlapping, inputs. If we are to use phase-resetting methods to analyze these circuits, we can either generate phase-resetting curves (PRCs) for all possible inputs and combinations of inputs, or we can develop an understanding of how to construct PRCs for arbitrary perturbations of a given neuron. The latter strategy is the goal of this study.

We present a geometrical derivation of phase resetting of neural limit cycle oscillators in response to short current pulses. A geometrical phase is defined as the distance traveled along the limit cycle in the appropriate phase space. The perturbations in current are treated as displacements in the direction corresponding to membrane voltage. We show that for type I oscillators, the direction of a perturbation in current is nearly tangent to the limit cycle; hence, the projection of the displacement in voltage onto the limit cycle is sufficient to give the geometrical phase resetting. In order to obtain the phase resetting in terms of elapsed time or temporal phase, a mapping between geometrical and temporal phase is obtained empirically and used to make the conversion. This mapping is shown to be an invariant of the dynamics. Perturbations in current applied to type II oscillators produce significant normal displacements from the limit cycle, so the difference in angular velocity at displaced points compared to the angular velocity on the limit cycle must be taken into account. Empirical attempts to correct for differences in angular velocity (amplitude versus phase effects in terms of a circular coordinate system) during relaxation back to the limit cycle achieved some success in the construction of phase-resetting curves for type II model oscillators. The ultimate goal of this work is the extension of these techniques to biological circuits comprising type II neural oscillators, which appear frequently in identified central pattern-generating circuits.

1 Introduction

In order to gain an understanding of the central pattern generators (CPG) involved in rhythmic motor activity such as locomotion (Arshavsky, Beloozerova, Orlovsky, Panchin, Yu, & Pavlova, 1985; Beer, Chiel, & Gallagher, 1999; Canavier et al., 1997; Chiel, Beer, & Gallager, 1999; Collins & Stewart, 1993; Collins & Richmond, 1994; Golubitsky, Stewart, Buono, & Collins, 1998) and respiration (Abramovich-Sivan & Akselrod, 1998a), it is necessary to understand the phase-resetting behavior of the neural oscillators that comprise such circuits. We have examined the structure of phase resetting in neural oscillators in order to construct phase-resetting curves (PRCs) in response to single and multiple perturbations of arbitrary amplitude and duration. Neural oscillators that produce periodic rhythms such as burst firing can be modeled effectively as limit cycle oscillators (Baxter et al., 2000), and such burst firing neurons are frequently components of CPGs (Chiel et al., 1999; Beer et al., 1999; Collins & Richmond, 1994; Kopell & Ermentrout, 1988). In this study, we ignore action potential generation and instead focus on the underlying oscillations whose plateaus comprise the bursts and whose troughs comprise the interburst hyperpolarizations. Since physiological inputs to real neurons in a CPG circuit frequently have a duration that is a significant fraction of the cycle period (Canavier, Baxter, Clarke, & Byrne, 1999), this work is a theoretical first step that will be extended to include inputs of significant duration.

A CPG is a network of neurons in the central nervous system that is capable of producing rhythmic output (Chiel et al., 1999; Beer et al., 1999; Golubitsky et al., 1998; Kopell & Ermentrout, 1988) in the absence of input from higher centers and sensory feedback. Networks of nonlinear oscillators have attracted a great deal of research due to their theoretical and practical importance (Canavier et al., 1999; Ermentrout, 1985, 1986, 1994; Izhikevich, 2000). When acting as a component of a network, nonlinear oscillators can be characterized by their PRC (Abramovich-Sivan & Akselrod, 1998a, 1998b; Dror, Canavier, Butera, Clark, & Byrne, 1999; Ermentrout, 1996; Pinsker, 1977). The PRC can be obtained by measuring the change in the period of the limit cycle when a pulselike perturbation is applied at different points in the cycle (phases). The power of PRC methods has been clearly demonstrated by Winfree (1980) and Murray (1993), as well as by Canavier et al. (1997, 1999). Most theoretical work on coupled oscillators has used normal form, or canonical reduction, methods (Ermentrout, 1994, 1996; Hoppensteadt & Izhikevich, 1997). However, such methods involve restrictive assumptions that can limit the application of these methods to circuits composed of physiological neurons. In this article, we explore the theoretical aspects of PRC construction that is based on a geometrical understanding of the phase-space dynamics as originally developed by Winfree (Glass & Mackey, 1988; Hoppensteadt & Izhikevich, 1997; Murray, 1993; Winfree, 1980) and does not require restrictive assumptions or any infor-

mation that cannot be easily obtained experimentally from physiological neurons.

A convenient way to study periodic behavior is to characterize a limit cycle oscillator by its phase. The term *phase* has been used in the literature in several different ways. Here we will use Winfree's definition (1980): the elapsed time measured from an arbitrary reference divided by the intrinsic period. We denote this term the temporal phase to distinguish it from the geometrical (or distance-based) phase defined below. In contrast to Winfree (1980), Murray (1993) and Hoppensteadt and Izhikevich (1997) defined the phase as the angle that parameterizes the unit circle. For a constant angular velocity on a circular limit cycle, the two definitions are equivalent. Given that limit cycles associated with nonlinear oscillators are usually not circular and can have highly variable angular velocity, we propose another definition that we call the geometrical phase. The geometrical phase can be defined as a distance measured from an arbitrary origin along the limit cycle divided by the intrinsic length of the limit cycle. Both definitions give quantities that are positive and normalized to unity. We stress that the temporally based definition of the phase (Winfree, 1980) has the same meaning as the distance-based one only for so-called phase oscillators, that is, the nonlinear oscillators running with a constant phase speed, or angular velocity.

As an illustrative example, we will use the Morris-Lecar oscillator, originally formulated to model action potentials in barnacle muscle (Morris & Lecar, 1981; Rinzel & Lee, 1986; Ermentrout, 1996). We will use it in a different context, as a model for the envelope of a burst-firing waveform described above. A limit cycle oscillation requires a minimum of two variables (Hoppensteadt & Izhikevich, 1997; Guckenheimer & Holmes, 1983; Murray, 1993; Winfree, 1980); in the Morris-Lecar model, these variables are membrane potential (V) and a negative feedback variable (w) that corresponds to a gating variable for an ionic channel. The limit cycle oscillator can exhibit a range of dynamic activity that depends on the characteristic timescales of the two variables (Rinzel & Lee, 1986; Rinzel & Ermentrout, 1998). If they are comparable in magnitude, the qualitative dynamics of a phase oscillator arise, and the two variables tend to vary smoothly in unison. If w varies much more slowly than V, a relaxation oscillator can be produced in which alternating rapid increases and decreases in V (*jumps*) are followed by slow relaxation in w. The qualitative characterization of a limit cycle oscillator as a phase oscillator, a relaxation oscillator, or an intermediate determines the relationship between time elapsed (temporal phase) and distance traversed along the limit cycle (geometrical phase). A mapping between geometrical phase and temporal phase was found to provide insight into the shape of the phase-resetting curve.

The Morris-Lecar model can exhibit two types of neural excitability. Neural excitability is the capability of a neuron to fire repetitively in response to an externally applied current. For type I excitability, the onset of repetitive firing occurs at arbitrarily low frequency, whereas for type II excitabil-

ity, the onset of repetitive firing occurs at a nonzero frequency (Hodgkin, 1948). The type of excitability is determined by the bifurcation structure: in type I, oscillations arise via a saddle node bifurcation, whereas in type II, they arise via a Hopf bifurcation (Rinzel & Ermentrout, 1998). The phase response characteristics of a neuron depend on the type of excitability it exhibits (Ermentrout, 1996): in general, type I neurons exhibit either only delays or only advances in response to perturbation of a given sign, whereas type II can exhibit both advances and delays to a given perturbation, depending on its timing. The phase response of the type I neuron is due to its essentially monotonic increase in membrane potential, except for a very rapid hyperpolarization phase of the action potential. Similar results apply to integrate-and-fire neurons for the same reason (Mirollo & Strogatz, 1990).

Our analysis assumed that for a neural oscillator, perturbations generally occur in the form of an increase or decrease in transmembrane current. The first derivative of membrane potential is proportional to the transmembrane current, whereas the transmembrane current does not appear in the derivatives of the other state variables, which for neural oscillators are generally gating variables. In oscillators in which the frequency of the temporal waveform is simply scaled by an increase in transmembrane current level, such as type I or integrate-and-fire models, the direction (advance or delay) of a brief perturbation can be determined using only the sign of the current perturbation and the sign of the first derivative of membrane potential (the instantaneous transmembrane current) at the time of the perturbation. By convention, a depolarizing (hyperpolarizing) current applied externally has a positive (negative) sign and produces a positive (negative) change or increase (decrease) in the membrane potential. Hence, if the signs are the same, there is an advance, whereas if they are different, there is a delay. For an ionic current, such as a synaptic current, the sign convention is opposite. Furthermore, the magnitude of the instantaneous geometrical phase shift due to a brief perturbation is proportional to the magnitude of the time integral of the perturbing current. Once the geometrical phase shift due to a perturbation has been calculated, the mapping from geometrical to temporal phase can be used to construct the desired PRC for oscillators. When

Figure 1: *Facing page*. Geometric versus temporal phase. Two-dimensional phase-space plot of the limit cycles for (A) a hypothetical phase oscillator, (C) Morris-Lecar (type I oscillator), and (D) FitzHugh-Nagumo (type II oscillator) relaxation oscillators. (B, D, F) The corresponding plots of the normalized geometrical distance (σ) versus temporal phase (ϕ). For a phase oscillator, the figurative point travels with constant angular velocity around the limit cycle, and therefore the normalized geometrical distance (σ) increases linearly (B). For the relaxation oscillators (D, F) the figurative point travels with variable speed along the limit cycle. (A) The four quadrants of a limit cycle; (F) the conversion from geometrical to temporal phase.

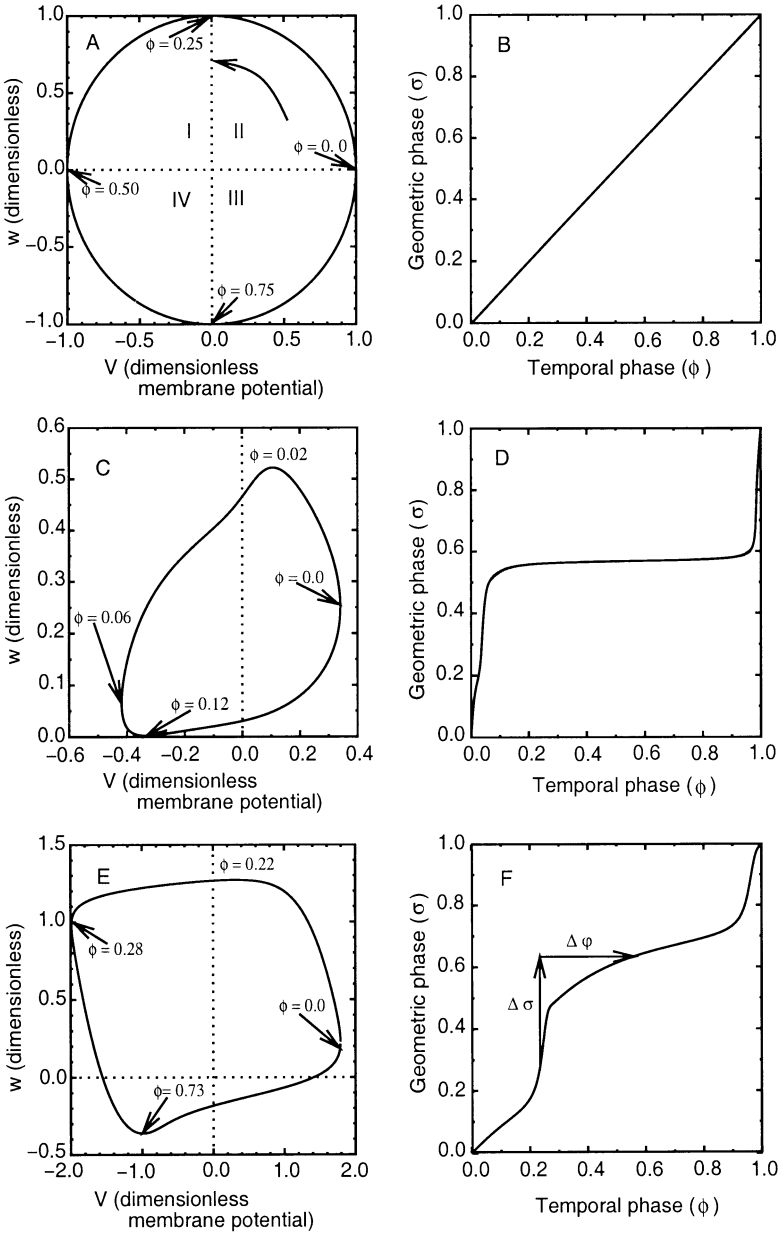

transmembrane current levels have more complex effects than simply scaling the frequency, additional calculations are required to compensate for effects on the amplitude of the temporal waveform.

2 A Geometric Analysis of Phase Resetting

2.1 A Mapping from Temporal to Geometrical Phase. The phenomenology of phase resetting can be best understood by visualizing a limit cycle, such as those shown in Figures 1A, 1C, and 1E, represented for convenience in a two-dimensional plane. Consider a system of N differential equations:

$$\frac{du_k}{dt} = f_k(u), \tag{2.1}$$

where $u_1 = V$. We used the infinitesimal Euclidean distance,

$$d\sigma = \sqrt{\sum_{k=1}^{N} (f_k(u))^2 dt}, \tag{2.2}$$

to define the geometrical phase along the limit cycle (Oprisan & Canavier, 2000a). Therefore, the length of a closed orbit is

$$L = \int_0^{P_i} \left(\sqrt{\sum_{i=1}^{N} (f_k(u))^2} \right) dt$$

where P_i is the intrinsic period of the motion. The normalized geometrical (distance-based) phase along a limit cycle is given by

$$\sigma = \frac{1}{L} \int_0^{t} \left(\sqrt{\sum_{k=1}^{N} (f_k(u))^2} \right) dt. \tag{2.3}$$

The geometrical phase σ is a monotonically increasing function of both the elapsed time t and the temporal phase $\phi = \frac{t}{P_i}$, where P_i is the intrinsic period of the limit cycle motion (see equations 2.3 and 3.2). The function $s(\phi)$ gives an invertible mapping between temporal and geometrical phase. Some examples of typical mappings are shown in Figures 1B, 1D, and 1F. For a phase oscillator, the geometrical and temporal phase are identical (see Figure 1B), whereas Figures 1D and 1F show that the mapping for relaxation oscillators can be highly variable and idiosyncratic.

A remarkable property of the geometrical to temporal phase mapping is its invariance. This mapping can be obtained using equation 2.3 if the evolution equations are known or by performing a time series delay embedding

to reconstruct the attractor (Takens, 1981; Abarbanel, Brown, Sidorowich, & Tsimring, 1993) first and then integrating along the numerically computed trajectory. We obtained a geometrical to temporal phase mapping for the Morris-Lecar model at the fixed parameter settings given in the caption of Figure 2. We used direct integration of the differential equations, as well as attractor reconstruction using delay embedding with two different delays, and in every case the agreement was very good (see Figure 2) (see appendix A for a detailed proof of invariance under certain assumptions).

2.2 Phase Resetting During a Perturbation. A geometrical perspective on phase resetting is given in Figure 3. A perturbation (the dark solid line in

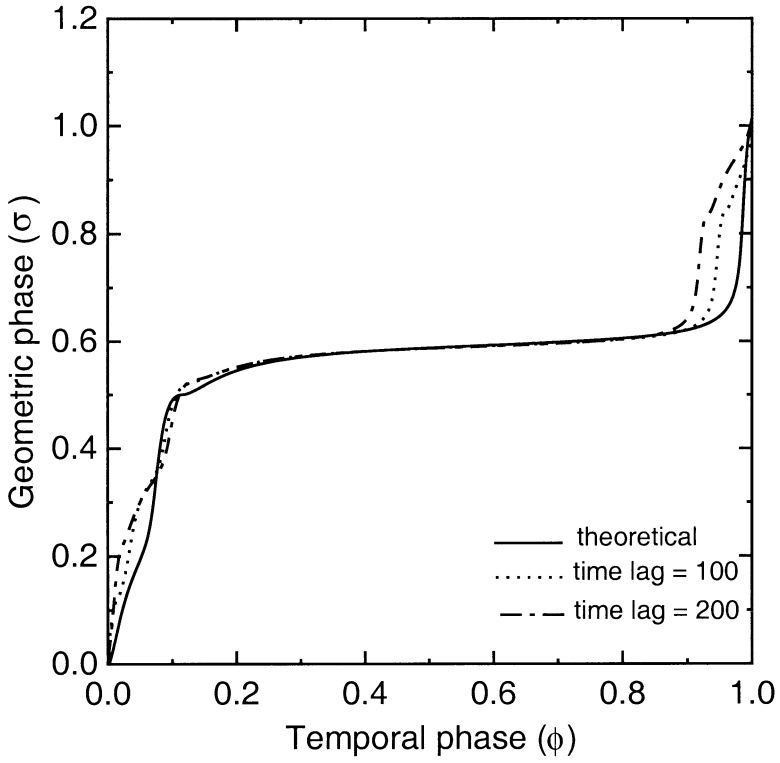

Figure 2: Dynamical invariance of the reconstructed geometrical to temporal phase mapping. The geometrical to temporal phase mapping was obtained by integrating the differential equations of the ML model oscillator in the type I excitability case. Using only the dimensionless membrane potential record, the phase-space attractor was reconstructed using two different time lags ($\tau = 100$, dotted line and $\tau = 200$, dot-dashed line), and for each reconstructed attractor, the geometrical to temporal phase mapping was computed.

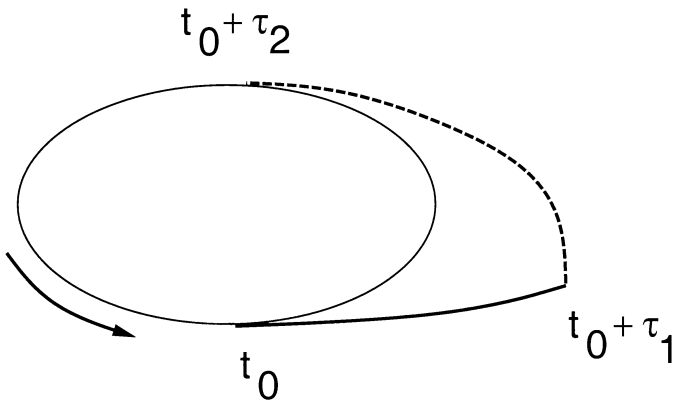

Figure 3: Topology of phase resetting. The phase-space plot of a two-dimensional stable limit cycle. A perturbation applied at time t_0 for a duration of τ_1 perturbs the trajectory (dark line). After the perturbation, the trajectory requires a time τ_2 to return to the limit cycle.

Figure 3) applied at time t_0 has a duration of τ_1. At the end of the perturbation, the trajectory may be at some distance from the limit cycle, and it relaxes back to the limit cycle (dashed line) during the time period τ_2. The temporal phase resetting is the normalized difference in elapsed time along the perturbed and unperturbed paths over the time period $\tau_1+\tau_2$. While τ_1 is easily determined, τ_2 is not. Fortunately, for the simple case of type I excitability, it is possible to neglect the resetting that occurs during τ_2, but we will first propose expressions that give the geometrical phase resetting for both τ_1 and τ_2 (see Oprisan & Canavier, 2001) and then recover the temporal phase resetting by using the inverse mapping from geometrical to temporal phase. The main idea is to obtain the projection of the perturbed trajectory onto the unperturbed trajectory. Physiological perturbations generally arise in the form of a perturbation in current, which affects only $\dot{V}$ or f_1 (see equation 3.1) and no other derivative (see also Nishii, 1999). The evolution equation of the membrane potential has the general form $\dot{V} = -\sum \frac{I_{ionic}}{C_m} + \frac{I_{ext}}{C_m}$, where $\sum I_{ionic}$ stands for the sum of all the ionic currents, C_m is the membrane capacitance, and I_{ext} is an externally applied current.

The projection of the vector representing the perturbation $(i(t)/C_m, 0, 0\ldots)$, where $i(t)$ is the perturbing current as a function of time, onto the vector containing the time derivatives $f_k(u)$ of the state variables evaluated along the limit cycle would produce the normalized infinitesimal distance traveled along the limit cycle:

$$d\sigma_1 = \frac{1}{L}\frac{i}{C_m}\frac{f_1(t)}{||f(t)||}dt. \tag{2.4}$$

Thus, the geometrical phase resetting during the perturbation of duration τ_1 would be

$$\Delta\sigma_1 = \frac{1}{L}\int_0^{\tau_1} \frac{i}{C_m}\frac{f_1(t)}{||f(t)||}dt. \tag{2.5}$$

If we assume that the perturbation has a very short duration, it is not necessary to integrate $\frac{f_1(t)}{||f(t)||}$ over the course of the perturbation; rather, we assume this quantity remains constant for the duration of the perturbation (Glass & Mackey, 1988; Guckenheimer & Holmes, 1983; Hoppensteadt & Izhikevich, 1997; Murray, 1993; Pavlidis, 1973). For simplicity of presentation, we assume that i is also constant for the duration τ_1 of the perturbation:

$$\Delta\sigma_1 = \frac{1}{L}\frac{\tau_1 i}{C_m}\frac{f_1(t_0)}{||f(t_0)||}. \tag{2.6}$$

Figure 4 illustrates the relationships among the vectors described above for a two-dimensional case for a phase advance in Figure 1A and a delay in Figure 1B. In each case, the vector s_0 represents the unperturbed limit cycle, the vector s^* represents the perturbed limit cycle, and Δs is the geometrical resetting before normalization by L, which then gives $\Delta\sigma_1$. The derivatives with respect to voltage are given by f_1 evaluated on the limit cycle at the point of the perturbation and by f_1^* during the perturbation. The derivative with respect to the second variable, f_2, is the same for the perturbed and unperturbed cases. The vectors are defined as follows: $\vec{s_0} = [\tau_1 f_1(t_0), f_2(t_0)]$ and $\vec{s^*} = [\tau f_1 + \Delta V, f_2(t_0)]$. The vector $\vec{s_0}$ would be traversed by the trajectory in the absence of a perturbation, and the vector $\vec{s^*}$ would be traversed in its presence. The direction of the perturbation is given by the difference $f_1^*\tau_1 - f_1\tau_1$, which is equal to $i\tau_1/C_m$, or ΔV. One can obtain the normal displacement Δh from the tangential displacement using similar triangles: $\Delta h = \frac{f_2(t_0)}{f_1(t_0)}\Delta\sigma_1$. This relationship becomes useful in the next section.

The temporal phase resetting is recovered using

$$\Delta\phi_1 = s^{-1}(\Delta\sigma_1). \tag{2.7}$$

The recovery can be accomplished graphically as shown in the lower portion of Figure 1F. The calculated $\Delta\sigma$ is added to the geometrical phase at the point at which the perturbation is received. The change in temporal phase is given by the horizontal displacement required to reach the new value of σ.

2.3 Phase Resetting During Relaxation Back to the Limit Cycle After a Perturbation. As shown in Figure 3, it is possible for the trajectory to be at some normal displacement from the unperturbed limit cycle after the perturbation has ended, so that additional phase resetting is incurred during τ_2, the relaxation back to the limit cycle. As we will show in the

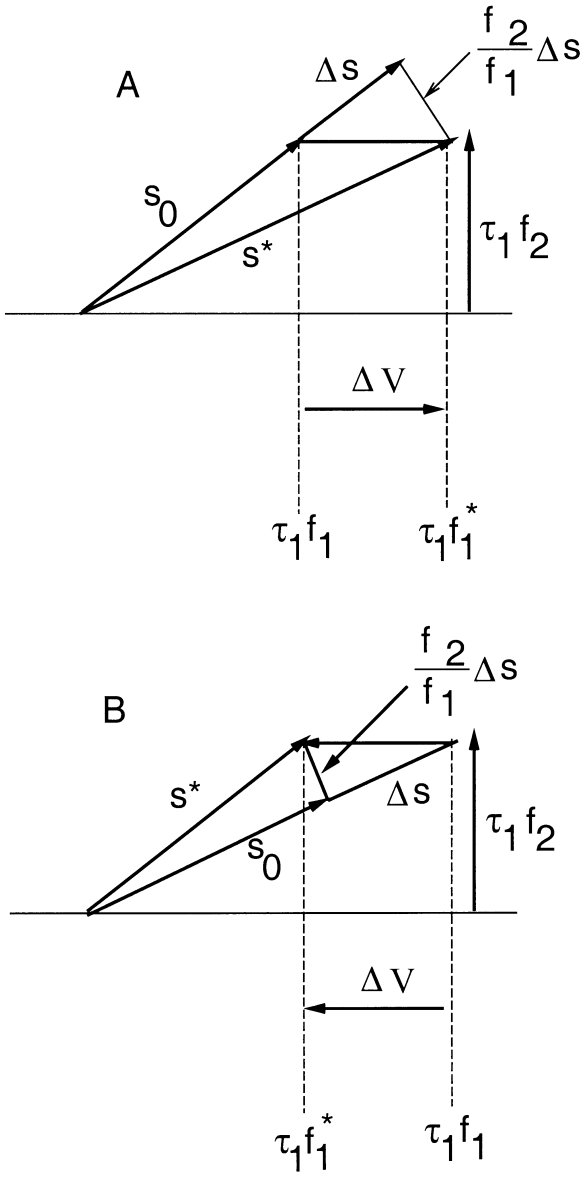

Figure 4: Idealized trajectory of a perturbation. The linearized tangent displacement along the unperturbed limit cycle s_0 and its perturbed counterpart s^*. The perturbed trajectory s^* is induced by a perturbation in transmembrane current: (A) the depolarizing case and (B) the hyperpolarizing case. The tangent geometrical phase shift Δs and the transverse displacement $\frac{f_2}{f_1}\Delta s$ can be easily written in terms of the unperturbed f and perturbed f^* vector fields.

Table 1: Phase Resetting Due to Normal Displacement from the Limit Cycle.

Quadrant	f_1	ΔV	$\Delta\sigma_1$	f_1/f_2	Δh		$\Delta\sigma_2$
I	−	−	+	+	+	Inside	+
		+	−	+	−	Outside	−
II	+	−	−	−	+	Inside	+
		+	+	−	−	Outside	−
III	+	−	−	+	−	Outside	−
		+	+	+	+	Inside	+
IV	−	−	+	−	−	Outside	−
		+	−	−	+	Inside	+

next section, for some types of oscillators, this additional phase resetting ($\Delta\sigma_2$ and $\Delta\phi_2$) can be neglected. For the case in which there is significant normal displacement that cannot be ignored, we have begun to calculate the appropriate corrections by initially assuming that the linear velocity of a trajectory just inside or just outside the limit cycle is approximately the same as that of a point on the limit cycle. However, in general, the angular velocity will be greater inside the limit cycle and smaller outside the limit cycle. Hence, trajectories that are horizontally displaced inside the limit cycle will be advanced, and those outside will be delayed. As a first approximation, we made the assumption that $\Delta\sigma_2$ is proportional to the normal distance Δh between the perturbed and unperturbed trajectories: $\Delta\sigma_2 = K\Delta h$. The normal distance can be calculated as

$$\Delta h = \frac{\left(\sqrt{\sum_{i=2}^{N}(f_k(u)^2}\right)}{f_1}\Delta\sigma_1. \tag{2.8}$$

For the two-dimensional case, the expression

$$\Delta h = \frac{f_2}{f_1}\Delta\sigma_1, \tag{2.9}$$

always gives the correct sign for the resetting. A limit cycle can be divided into four quadrants (see Figure 1A): in I, $f_1 < 0$ and $f_2 < 0$, in II $f_1 > 0$ and $f_2 < 0$, in III $f_1 > 0$ and $f_2 > 0$, and in IV, $f_1 < 0$ and $f_2 > 0$. The sign of $\Delta\sigma_1$ is given by $sgn(f_1\Delta V)$, and the sign of $\Delta\sigma_2$ is given by $sgn(\frac{f_2}{f_1}\Delta\sigma_1)$, and in every case, a normal displacement outside the limit cycle gives a positive $\Delta\sigma_2$, which corresponds to an advance, and a displacement inside the limit cycle gives a negative $\Delta\sigma_2$, or a delay (see Table 1).

The remaining problem is to assign a value to the proportionality K. The constant of proportionality K between the normal displacement and its corresponding additional tangential displacement was found by calculating the time required for relaxation to the limit cycle, assuming the temporal

phase resetting was proportional to the relaxation time, and converting this temporal resetting to geometrical resetting and finding the appropriate K. First, we determined the maximum normal distance ($\Delta h_{\max}$) between the unperturbed limit cycle and a perturbed limit cycle with a current perturbation of i. The normalized time $\Delta\phi_{\max}$ (with respect to the intrinsic period of the unperturbed limit cycle) necessary for the figurative point to relax from the maximum displacement sufficiently close to the unperturbed limit cycle was determined. $\Delta\phi_{\max}$ was converted to $\Delta\sigma_{\max}$ using the temporal to geometrical mapping. The constant K is the ratio $\Delta\sigma_{\max}/\Delta h_{\max}$. Since the time required to relax back to the limit cycle (τ_2 in Figure 3) is theoretically infinite, we used instead the time required to relax to within a neighborhood of the limit cycle defined by the limits of our computational accuracy (Izhikevich, 2000). A plot of the natural logarithm of normal displacement versus time (not shown) was linear until this limit was reached; then it became flat. The time to reach the end of the linear region was normalized to give $\Delta\phi_{\max}$.

Once again, the temporal phase resetting is recovered as

$$\Delta\phi_2 = s^{-1}(\Delta\sigma_2), \tag{2.10}$$

and the total phase resetting is given by $\Delta\phi = \Delta\phi_1 + \Delta\phi_2$.

3 Results Using the Morris-Lecar Model as an Example

The Morris-Lecar model has the advantages of simplicity (it has only two state variables) and versatility (it can exhibit either type I or type II excitability, depending the values of its parameters). We used the following general dimensionless form of the nonlinear oscillator,

$$\dot{V} = f(V, w) + I_{ext} = f_1(V, w; I_{ext}),$$

$$\dot{w} = g(V, w) = f_2(V, w; I_{ext}), \tag{3.1}$$

where V stands for the fast variable, w for the slow variable, and I_{ext} for the control parameter (external applied current). Two-dimensional reduced models like Morris-Lecar (Morris & Lecar, 1981; Ermentrout, 1994) and FitzHugh-Nagumo (FitzHugh, 1969) have similar dimensionless forms.

The ionic currents can be written in terms of membrane potential V and slow variable(s) (see appendix B). The expression for geometrical phase resetting due to tangential displacement during a perturbation (see equation 2.6) becomes

$$\Delta\sigma_1 = \frac{1}{L}\frac{\tau_1 i}{C_m}\frac{f_1(t_0)}{\sqrt{f_1(t_0)^2 + f_2(t_0)^2}}, \tag{3.2}$$

where $f_1 = \dot{V}$ and $f_2 = \dot{w}$.

In order to evaluate the success of our methods for constructing the PRC using the methods described in the preceding section, we numerically generated actual PRCs for the Morris-Lecar model using an explicit fourth-order Runge-Kutta method to solve the nonlinear equations B.1. The simulations were compiled on C/UNIX and run on a Sun Enterprise 450 Ultra Server. First, the differential equations were numerically integrated for until the solution converged to the limit cycle and the period P_i of the steady solution was computed. Then a steplike current pulse was applied at different temporal phases (ϕ) during the cycle with respect to an arbitrary fixed reference point on the limit cycle (we used the maximum of the membrane potential as a reference point, but different points can be used Canavier et al., 1997, 1999). The perturbed period P of the membrane potential is measured, and the quantity $F(\phi) = P/P_i - 1$ is computed for each value of ϕ. $F(\phi)$ was used for consistency with our previous articles and is equal to $-\Delta\varphi$. These actual PRCs were used for comparison with the theoretical PRCs. For precise continuity near the reference point, the second perturbed period after the pulse is applied should also be tabulated and the effect on both periods summed to produce $F(\phi)$ (Canavier et al., 1997, 1999), but the second perturbed pulse was not examined in this article.

3.1 Phase Resetting Induced in Type I and Type II Oscillators by a Single Input. The actual PRC for a type I oscillator (parameters given in appendix B) receiving an excitatory input is shown in Figure 5A (dotted line), and compared with the PRC constructed according to the methods described in the preceding section (dashed line). Only the contribution from $\Delta\sigma_1$ was included in the calculation; any contribution from $\Delta\sigma_2$ was neglected. It can be seen from the common plot of actual and predicted PRCs result that our geometrical method gives a very good estimation of the PRC for the type I oscillator. As we expected, based on analytic results (see equation 3.2), the amplitude of the PRC is proportional to pulse duration τ_1 (see Figure 5B) and also to the pulse amplitude as shown in Figure 5C. The shape of the geometrical phase shift curve can be anticipated by examining equation 3.2 together with the waveform of the membrane potential (see Figure 6C). Since the membrane potential is always increasing except in a very short time interval, we would expect a depolarizing external stimulus to produce a negative phase shift (an advance), as is indeed the case in Figure 5A. However, this is a very small temporal window in which the membrane potential is decreasing, and a perturbation applied at this time would produce a phase shift of the opposite sign. As a practical matter, such an anomalous phase shift would be difficult to observe in a physiological type I oscillator, but in a model, we have the precision to detect it. Hence Figure 7 illustrates how this region of anomalous phase shift narrows as the bifurcation that generates type I excitability is approached. A numerical computation of the ratio of time interval during which the membrane potential is decreasing to the period of the signal is shown in Figure 7. The time

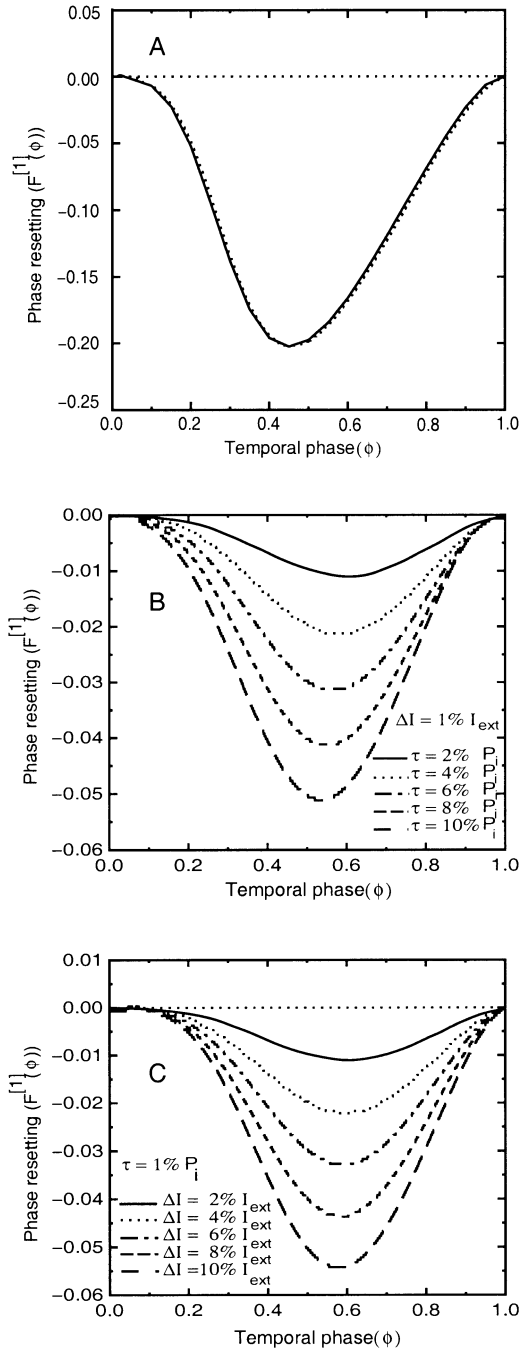

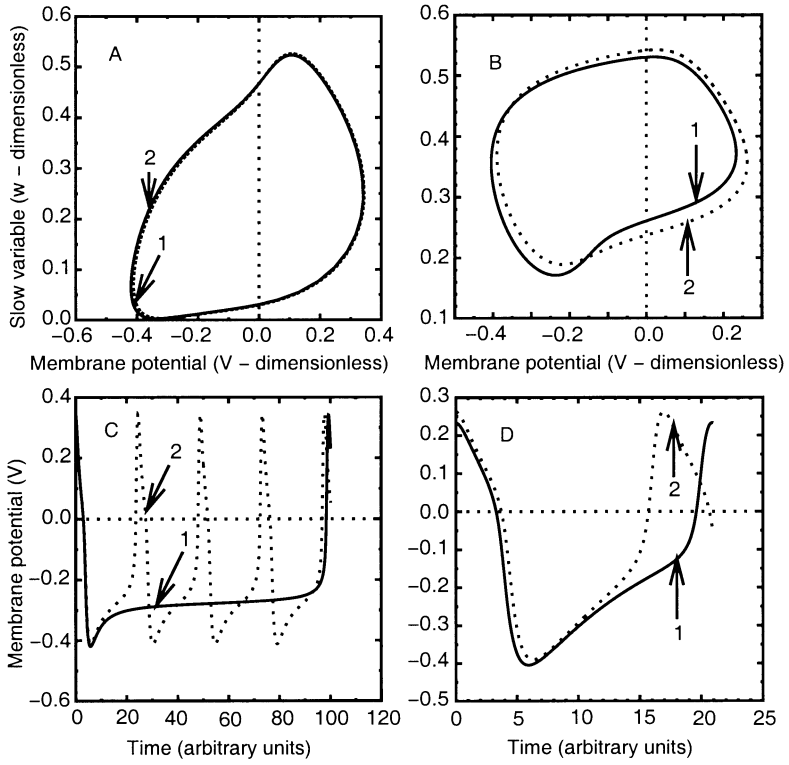

Figure 6: Effect of bias current on limit cycle topology and angular velocity (frequency). Two-dimensional limit cycles for (A) Morris-Lecar type I and (B) type II excitability cases. The curves labeled 1 and 2 were obtained at different values of I_{ext}. For type I excitability, the topology of the attractor is not very sensitive to changes in the control parameter I_{ext} (A), whereas the period of the limit cycle motion is sensitive to the same change in I_{ext} (C). On the other hand, the topology of the attractor obtained via a type II excitability mechanism (Hopf bifurcation) is dramatically influenced by a change in the control parameter I_{ext} (B) but the period is not (D).

Figure 5: *Facing page*. Predicted (analytic) versus actual (numerically computed) type I phase resetting. (A) The numeric (continuous curve) and analytically mapped (dotted curve) PRCs for type I excitability case. Perturbation duration was $\tau = \frac{P_i}{100}$ using equation 3.2 and the graphic mapping procedure. The steady dimensionless current was $I_{ext} = 0.0695$, and the pulse amplitude was 10% of I_{ext}. A summary of numerical simulations confirms that the PRC amplitude scales with the product of current amplitude (B) and its duration (C) as theoretically predicted by the equation 3.2.

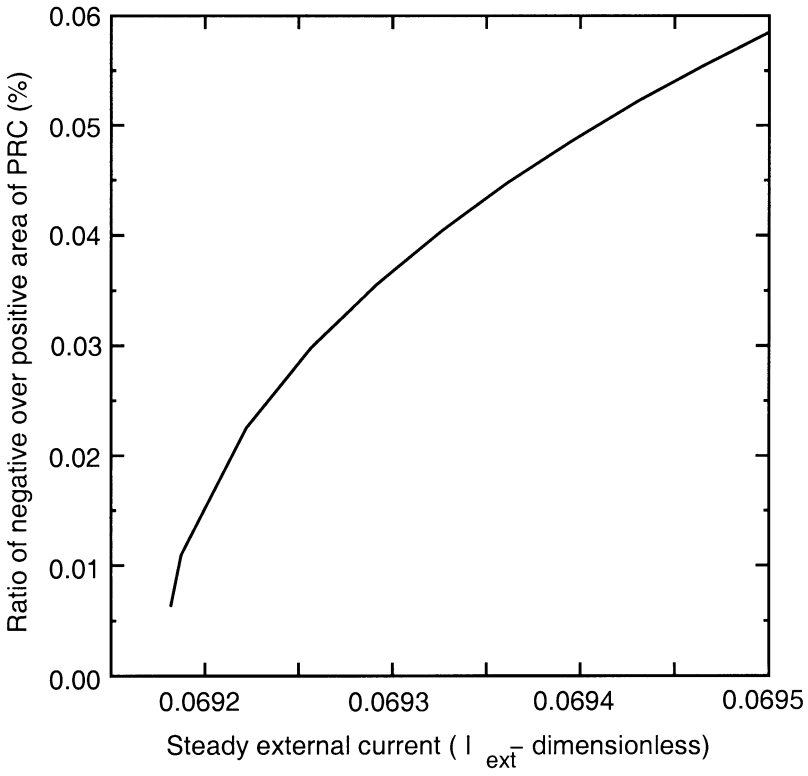

Figure 7: Deviation of type I model from resetting curve with a single sign. The deviation is plotted as the fraction of the cycle over which the phase resetting has the opposite sign from the idealized type I PRC, in which all phase resets in response to a given input have the same predictable sign. When the control parameter approaches the bifurcation point (criticality), the relative magnitude of the time interval over which the membrane potential decreases becomes negligible.

interval over which the membrane potential decreases from its maximum to minimum is almost constant over a very large control parameter range, but as the bifurcation (criticality) is approached, the period increases, so the ratio decreases. Theoretically, in the limiting case of criticality, the period of the membrane potential oscillation becomes infinite because the phase trajectory approaches the separatrix. On the other hand, using our observation that the time interval over which the membrane potential decreases from its maximum to minimum is nearly constant over a very large range of I_{ext} and Ermentrout's (1996) formula for the period of the membrane oscillations $T \propto (I_{ext} - I_c)^{-1/2}$, where I_c is the critical value of the control

parameter at the saddle-node bifurcation point, it is possible to derive an analytic expression for the plot in Figure 7. Therefore, the computational determined ratio can be satisfactorily fitted by $\sqrt{(I_{ext} - I_c)}$. These two observations lead to the conclusion that the relative magnitude of positive part of PRC (which is related to the relative contribution of the decreasing membrane potential to the whole signal duration) decreases to zero as we approach criticality. Rinzel and Ermentrout (1998) make the same point: "In only a very small interval of time can the phase be delayed, and this is a general property of membranes that become oscillatory through a saddle node bifurcation" (p. 286).

The temporal waveform given in Figure 6C explains the general shape of the PRC, and the effect of a perturbation in current on both the phase plane representation (see Figure 6A) and the temporal waveform (see Figure 6C) explains why the phase resetting due to relaxation after a normal displacement is not significant for oscillators that exhibit type I excitability. An important topological feature of the associated limit cycle attractor shown in the phase-plane representation of Figure 6A is its invariance with respect to change in the applied current. On the other hand, the period of the limit cycle motion is highly sensitive with respect to such changes (see Figure 6C). For type I excitability, a perturbation in current produces a negligible normal displacement from the limit cycle. Therefore, in this case, the geometrical phase difference occurs solely because of different speeds of the figurative points along the limit cycle. Quantitatively, the normal displacement from the unperturbed limit cycle is proportional to $\frac{f_2(t_0)}{f_1(t_0)}$. For the type I oscillators that we examined in this study, we found that the average value of the above ratio is about $2.8\,10^{-4}$ using the dimensionless (normalized) forms of V and w, whereas for type II oscillators, the average value was 2.8. Thus, the normal displacement induced by the same perturbation is four orders of magnitude smaller for type I oscillators than for type II oscillators. This explains the excellent results using only $\Delta\sigma_1$ representing tangential displacement during a perturbation for type I. Since the normal displacement is significant for type II oscillators (see Figure 6B), we expect that we will have to include the contribution $\Delta\sigma_2$ from relaxation after normal displacement.

Type II excitability arises via a Hopf bifurcation. In contrast to type I excitability, the geometry of the associated limit cycle attractor is very sensitive to control parameter changes (see Figure 6B), but the period of the motion changes more slowly than for type I excitability (see Figure 6D). As we expected, calculating the PRC using only the contribution of $\Delta\sigma_1$ (dotted line, Figure 8A) did not produce a good fit to the actual PRC. For the two-dimensional case, the expression for $\Delta\sigma_2$ becomes

$$\Delta\sigma_2 = K\frac{f_2(t_0)}{f_1(t_0)}\Delta\sigma_1, \tag{3.3}$$

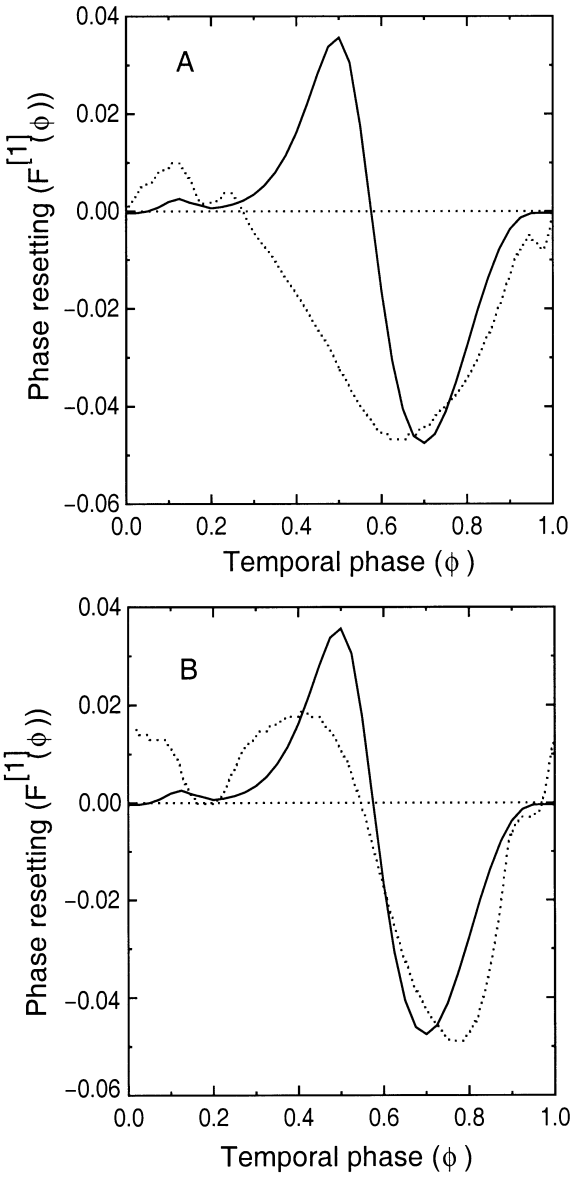

for type II parameter settings (given in appendix B). Adding the contributions of both $\Delta\sigma_1$ and $\Delta\sigma_2$ produced a better fit (see Figure 8B), but not the nearly perfect agreement achieved for type I. Possible future directions for improving the fit are given in section 4.

3.2 Phase Resetting Induced in a Type I Oscillator by Multiple Inputs per Cycle. We generalized the above methodology to the case in which the neural oscillator receives more than one input during a cycle (Oprisan & Canavier, 2000b). Only the simpler case of type I excitability is addressed so that we could assume the trajectory returns to the limit cycle between successive perturbations. We considered the simplified case of two identical current pulses, meaning that $\tau_1 = \tau_2$ and $\Delta I_{ext\,1} = \Delta I_{ext\,2}$ (see Figure 9A). Here, τ_1 and τ_2 denote the duration of two distinct pulses rather than the duration of the perturbation and the associated relaxation back to the limit cycle as in the preceding sections. t_1 denotes the time at which the first pulse current is applied (see Figure 9A). As a consequence of this current perturbation, the geometrical phase shift induced at time t_1 is given by the equation 3.2. Another current pulse is applied at time t_2. The geometrical phase shift is again given by equation 3.2, but the temporal phase at which the second pulse is applied is $t_1/P_i + \Delta\phi_1$, where $\Delta\phi_1$ is the temporal phase shift corresponding to the geometrical phase shift previously determined for the first pulse. Therefore, if we denote by $F^{[1]}(\phi)$ the single-pulse PRC as it was defined in the preceding section, then for two identical current pulses acting during the same cycle, the PRC becomes

$$F^{[2]}(\phi) = F^{[1]}(\phi) + F^{[1]}\left(\phi + F^{[1]}(\phi) + \frac{t_2 - t_1}{P_i}\right), \tag{3.4}$$

where P_i is the intrinsic period of the oscillation for the steady external current value $I_{ext\,1}$ and $\frac{\tau_1+\tau_2}{P_i} < 1$ in order to deliver both the current pulses during the same cycle (Ermentrout & Kopell, 1991b). This analysis also can be generalized to more than two inputs per cycle with arbitrary amplitude-duration ratios. We performed extensive numerical simulations to verify our predictions using a Morris-Lecar model neuron. Figure 10 summarizes the agreement between the predicted two-pulse PRC (continuous curve)

Figure 8: *Facing page*. Predicted (analytical) versus actual (numerically computed) type II phase resetting. (A) Uncorrected and (B) corrected for relaxation numeric (continuous curve) and analytic (dotted curve) PRCs for type II excitability. The duration of the perturbing pulse was $\tau = \frac{P_i}{100}$. The steady dimensionless current was $I_{ext} = 0.25$, and the pulse amplitude was 10% of I_{ext}. This anomalous region is given due to the finite cycle fraction during which membrane potential is rapidly decreasing, whereas it increases during the remainder of the cycle.

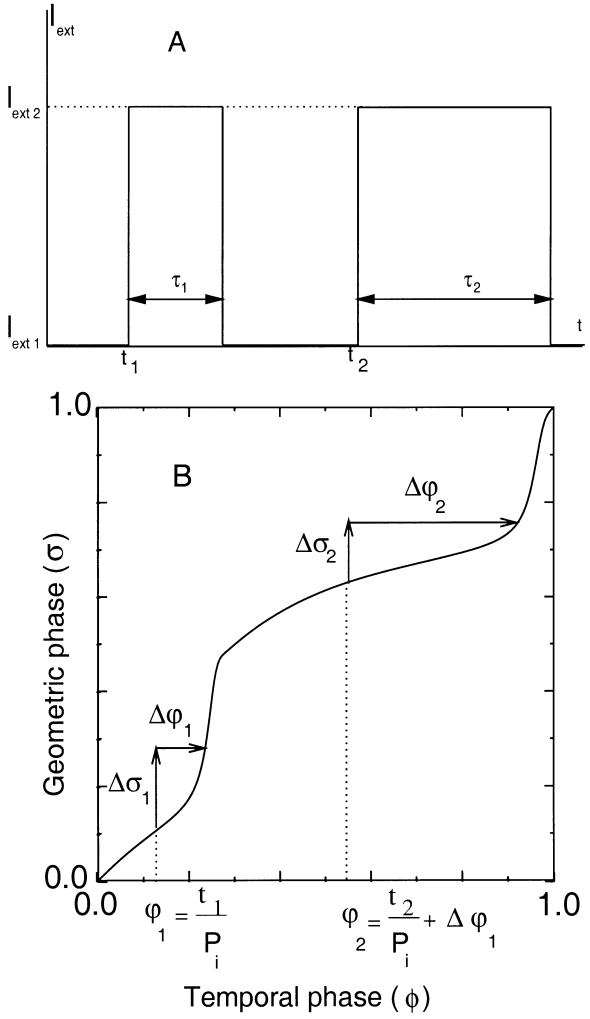

Figure 9: Generalization of the resetting topology to multiple pulses. (A) Two brief current pulses with the same amplitude $\Delta I_{ext} = I_{ext\,2} - I_{ext\,1}$ and duration $\tau_1 = \tau_2$ acting during the same cycle. (B) The figurative point is accelerated along the unperturbed limit cycle when perturbation is first applied (t_1) for the interval τ_1. When the first perturbation switches off, the figurative point again moves along the unperturbed limit cycle until a second pulse is applied, at time t_2. The figurative point is again accelerated along the limit cycle and moves along it. When the second perturbation terminates, the figurative point again moves along the unperturbed limit cycle. Mapping the geometrical phase differences into temporal phase differences, we found the PRCs for multiple inputs per cycle (see B).

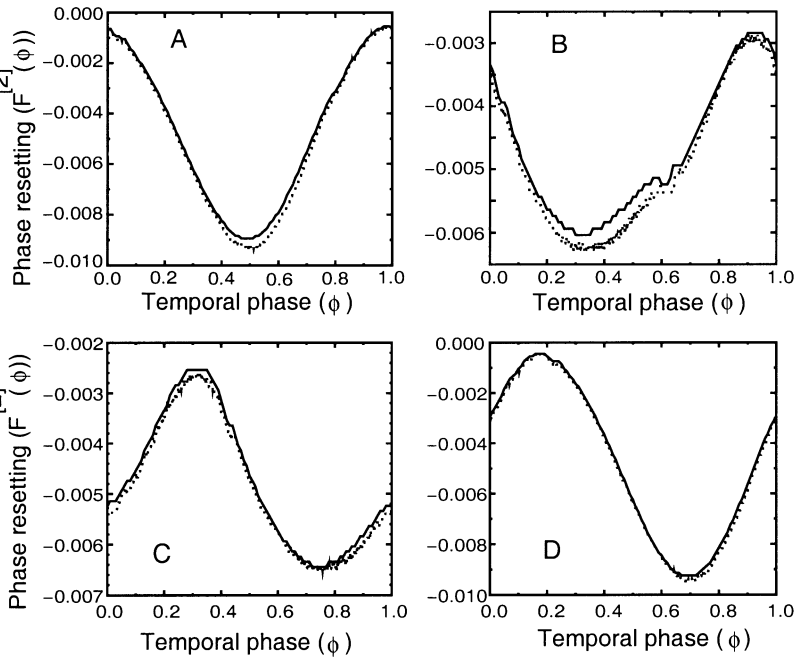

Figure 10: Predicted versus actual phase resetting for multiple pulse protocol. Common plot of predicted (continuous line) and actual numerically computed (dotted line) PRCs with two identical current pulses applied during the same cycle. The pulse's amplitude was 1% of the steady external current, and its duration was 1% of the intrinsic period P_i. The only variable was the distance between current pulses: (A) 20%P_i, (B) 40%P_i, (C) 60%P_i, and (D) 80%P_i.

and its numerically computed actual counterpart (dotted curve) for variable distances between the two current pulses. The agreement between the actual and predicted values is very good. We also found that the shape of the current pulse is not critical. Numerical simulations using a presynaptic input from an identical Morris-Lecar model neuron rather than a square pulse gave results in agreement with equation 3.4. Another recent study (Foss & Milton, 2000) also showed that the shape of the presynaptic input does not dramatically change the response of the postsynaptic neuron.

4 Discussion and Conclusion

The improvement of the theoretical understanding of the PRC is significant. First, we used an unambiguous definition of geometrical (distance-based) phase that applies for every nonlinear oscillator even in high-dimensional spaces. Second, we provided a geometrical conceptual basis for phase reset-

ting. The phase-space analysis that we performed revealed complex problems posed by phase-resetting mechanisms and suggested analytic approaches in order to solve these problems. A main result of this article is a general method that allows the analytic construction of the PRC in addition to previously established computational methods. The relationship of our approach to previous approaches to this problem is given in appendix C. Although we referred to a particular model (Morris-Lecar) in order to compare our findings with numerically reported ones, the method we described is generally applicable. The theoretical predictions have been confirmed by numerical solution. For type I excitability, the agreement is quite satisfactory and generalizes to any arbitrary combination of pulses. For type II excitability, some disagreement persists, and further theoretical work is required. One source of error in the prediction of type II PRCs is the uncertainty in the tangential displacement due to relaxation after normal displacement. This tangent displacement was assumed to be linearly proportional to the normal displacement. However, for a very simple circular limit cycle with radius r_0 and a constant angular velocity at all points on the limit cycle and a constant linear velocity at all points near the limit cycle, it can be shown that a normal displacement of Δr produces a tangential displacement proportional to $\ln(\frac{r_0+\Delta r}{r_0})$. Since limit cycles are not in general circular, the quantities r_0 and Δr are not defined for arbitrary limit cycles such as those shown in Figure 6. Nevertheless, perhaps a better approximation of the dependence of tangent displacement (geometrical phase) on normal displacement can be made by defining analogous quantities for arbitrary limit cycles.

The ultimate goal of this work is to apply the results to the analysis of circuits composed of physiological oscillators, including bursting neurons. The fundamental assumption of phase-resetting analysis is that the only effect of a perturbation is to lengthen or shorten the cycle in which a perturbation is received. When a neuron is a component of a network, the burst in that component neuron serves as the perturbation received by the neurons on which it makes synaptic connections. Thus, an alteration in burst duration or amplitude may have an impact on the resetting induced in the target neurons. To measure the magnitude of the signal shape change induced by perturbation, we evaluated the relative change in the maximum amplitude of the signal. For type I excitability, the maximum amplitude of membrane potential is negligibly affected by perturbations, as one would expect from the coincidence of perturbed and unperturbed limit cycles. However, burst duration may be affected. Similarly, again as one would expect, for type II excitability, we observed that the maximum amplitude of the membrane potential significantly changes in a manner strongly correlated with the PRC. Preliminary work (Oprisan & Canavier, 2000a, 2000b) shows that these effects of perturbations do not significantly compromise our ability to analyze circuits of coupled Morris-Lecar oscillators using their PRC characteristics. The work presented in this article will help us to analyze physiological cir-

cuits without having to generate PRCs experimentally in every combination of number, timing, amplitude, and duration of perturbations that might result from the oscillatory activity of the circuit, but rather to generalize from a small number of PRCs, we hope as few as one per neuron.

How can this method be extended to physiological neurons? Although we do not have access a priori to the equations that govern the electrical activity of a given neuron, this method can still apply to physiological neurons because we have observed that the geometrical to temporal phase relationship that we obtained here using equation 2.3 is similar to that we can numerically extract using membrane potential record. More generally, we can replace the described Euclidean-based approach (which requires analytic expressions of the vector field) by a computational geometrical phase construction based entirely on a delayed embedding using the fast variable record (Takens, 1981). In order to obtain a slow variable, filtering techniques may be required. Once we have obtained an appropriate phase-plane reconstruction, the geometrical to temporal phase mapping can be obtained and then the predicted phase resetting induced by external perturbations. We predict (Oprisan & Canavier, 2000a, b) that these two steps can give us the PRC for neurons (such as cortical neurons) that are type I oscillators (Wilson & Bower, 1989; Traub & Miles, 1991). Experimentally obtained PRCs can then be used to confirm the validity of our theoretical analysis. In addition, these methods can be extended to type II neural oscillators, which appear frequently in physiological central pattern generators, by experimentally estimating the proportionality constant K to correct for phase resetting that occurs during relaxation after normal displacement from the limit cycle.

Appendix A: The Dynamical Invariance of the Mapping Between the Geometrical Phase and the Temporal Phase

The dynamical invariance of the geometrical to temporal phase curve, which is a homeomorphism from the limit cycle to unit circle, is especially important for our short-term objective, which is the recovery of the PRC from a phase-space reconstruction of the attractor. The sketch of the proof that the geometrical to temporal phase curve is an invariant is as follows. Consider a one-dimensional time series, such as the membrane potential record, for example.

$$x[1], x[2], x[3], \ldots, \tag{A.1}$$

where the $x[i]$ are evenly sampled at intervals of Δt, the time delay τ is an integral multiple of Δt, and D is the embedding dimension of the appropriate phase space. Then the following D-dimensional vectors describe the attractor:

$$y[i] = x[i], x[i+\tau], x[i+2\tau], \ldots, x[i+(D-1)\tau]. \tag{A.2}$$

The Euclidean distance between two successive points $y[i]$ and $y[i+1]$ along the reconstructed attractor is

$$R^2_{i,i+1}(D) = \sum_{k=0}^{D-1} (x[i+1+k\tau] - x[i+k\tau])^2, \tag{A.3}$$

which gives for the length of the closed trajectory $L(D) = \sum_{i=1}^{N} R_{i,i+1}(D)$, where N is the number of points along the closed trajectory and $x[i] = x[i+N]$. The geometrical distance (before normalization) after $j < N$ steps along the limit cycle is

$$s_j(D) = \sum_{i=1}^{j} R_{i,i+1}(D). \tag{A.4}$$

Let D be the minimum embedding dimension of the attractor. Reconstructing the attractor in 2D-dimensional phase space, we obtain:

$$R^2_{i,i+1}(2D) = \sum_{k=0}^{2*D-1} (x[i+1+k\tau] - x[i+k\tau])^2. \tag{A.5}$$

This can be rewritten as:

$$R^2_{i,i+1}(2D) = \sum_{k=0}^{D-1} (x[i+1+k\tau] - x[i+k\tau])^2 + \sum_{k=D}^{2D-1} (x[i+1+k\tau] - x[i+k\tau])^2$$

$$= R^2_{i,i+1}(D) + \sum_{j=0}^{D-1} (x[i+1+(D+j)\tau] - x[i+(D+j)\tau])^2$$

$$= R^2_{i,i+1}(D) + \sum_{j=0}^{D-1} (x[i+1+D\tau+j\tau] - x[i+D\tau+j\tau])^2. \tag{A.6}$$

The lag time τ should be as small as possible to capture the shortest changes in the data, yet it should be large enough to generate the maximum possible independence between the components of the vectors in the phase space.

Since the time span $D\tau$ of each vector in the phase space represents the duration of a state of the system, it should be at most equal to the period of the dominant frequency $D\tau = N$ (both τ and N are integer multiples of the time step Δt). Therefore, $x[i+D\tau] = x[i+N] = x[i]$, where the last equality

means that the period of the attractor is N. Using the above observation, the above expression simplifies to

$$R^2_{i,i+1}(2D) = 2R^2_{i,i+1}(D). \tag{A.7}$$

Thus, the geometrical distance $s_j(D)$ after j steps along the limit cycle and the total length of the limit cycle $L(D)$ show the same scaling with respect to the embedding dimension: $\frac{s_k(2*D)}{L(2*D)} = \frac{s_k(D)}{L(D)}$. Our numerical computations show that the general scaling relationship is $s_k(\alpha * D) = s_k(D)(\alpha)^\gamma$ with γ slowly dependent on k with a saturation threshold $\gamma \simeq .5$, which also supports our conjecture that the mapping between geometrical and temporal phase is a dynamical invariant.

Appendix B: The Dimensionless Morris-Lecar Model Neuron

We use the Morris-Lecar model as an example of a simple neural model. Despite its simplicity, it produces a facsimile of the membrane potential envelope of a neural oscillator. The dimensionless equations are (Morris & Lecar, 1981; Rinzel & Lee, 1986; Rinzel & Ermentrout, 1998):

$$\frac{dV}{dt} = I_{ext}(t) - g_{Ca}m_\infty(V)(V - V_{Ca}) - g_K w(V - V_K) - g_L(V - V_L) = f_1(V, w),$$

$$\frac{dw}{dt} = \phi\lambda(V)\,(w_\infty(V) - w) = f_2(V, w), \tag{B.1}$$

with $m_\infty(V) = \frac{1}{2}\left(1 + \tanh\left(\frac{V-V_1}{V_2}\right)\right), w_\infty(V) = \frac{1}{2}\left(1 + \tanh\left(\frac{V-V_3}{V_4}\right)\right), \lambda(V) = \cosh\left(\frac{V-V_3}{2V_4}\right)$.

For type I excitability, we have (Rinzel & Ermentrout, 1998) the following values: $V_1 = -0.01$; $V_2 = 0.15$; $V_3 = 0.1$; $V_4 = 0.145$; $V_K = -0.7$; $V_L = -0.5$; $V_{Ca} = 1.0$; $g_{Ca} = 1.33$; $g_K = 2.0$; $g_L = 0.5$; $\phi = 0.33$; $I = 0.0705$.

For type II excitability, the parameters have the same values except $V_3 = 0.017$; $V_4 = 0.25$; $g_{Ca} = 2.2$; $g_K = 4.0$; $g_L = 1.0$;$\phi = 0.4$; $I = 0.4$.

Appendix C: Comparison with Previous Studies

There are similarities between our method of predicting phase resetting and those given in the appendix of Ermentrout and Kopell (1991a, b), but there are some significant differences as well. Our derivation uses geometrical intuition, whereas that of Ermentrout and Kopell is analytic. In Ermentrout and Kopell (1991a, b), a system of N state variables representing oscillator k that is coupled to oscillator j as a function of time,

$$\frac{du_k}{dt} = f_k(u_k) + g(u_k, u_j), \tag{C.1}$$

is converted by a change of variables to a system that is a function of phase (θ) around the limit cycle solution to the original equations, as well as $N-1$ variables that measure normal distance from the limit cycle. These latter $N-1$ variables can be ignored by assuming a strong attraction to the limit cycle, which renders these $N-1$ variables negligibly small (as in a type I oscillator). Ermentrout and Kopell further assume that the phase variables of two coupled oscillators are never perturbed independently, which reduces the system to a single phase variable. The vector $U_k^{'}$ contains the derivatives evaluated along the limit cycle of each of the original state variables with respect to phase ($dU_k/d\theta$):

$$w\frac{du_k}{dt} = U_k^{'}(\theta)\frac{d\theta_k}{dt}, \tag{C.2}$$

where $\theta(t) = wt$ and $d\theta = wdt$. Combining equations C.1 and C.2 yields

$$w^{-1}U_k^{'}(\theta)\frac{d\theta_k}{dt} = f_k(U_k) + g(U_k, U_j). \tag{C.3}$$

Multiplying both sides of the equation C.3 by the inverse of $U_k^{'}$, which is $U_k^{'T}/||U_k^{'}||^2$ and using the fact that $f_k(U_k) = U_k^{'}(\theta(t))$, the following expression results:

$$\frac{d\theta_k}{dt} = w + w\frac{U_k^{'}}{||U_k^{'}||^2}g(U_k, U_j). \tag{C.4}$$

A similar expression appears in Hoppensteadt and Izhikevich (1997, p. 255).

By analogy with equation A4 of Ermentrout and Kopell (1991a, b), we can define $h_k(\theta_k, \theta_j)$ as $\frac{U_k^{'}}{\rho_k}g(U_k, U_j)$. Both our derivation and that of Ermentrout and Kopell (1991a, b) take advantage of the fact that the coupling is in one variable (V) only, hence for the particular form of perturbation. They assumed in a system of two coupled Morris-Lecar oscillators:

$$g(U_k, U_j) = [g_{ex}(V_k(\theta)(V_{ex} - V_j(\theta)), 0]. \tag{C.5}$$

The nonzero term is simply the scaled instantaneous current and is equivalent to the scaled instantaneous current in our derivation, I/C_M. We assumed a constant pulse, but any arbitrary pulse can be used, and the integral of that scaled current over the perturbing pulse can be substituted for $(I\tau)/C_M$, or ΔV, in our formulation.

Thus, the final expression to be used for comparison with our results is

$$\frac{d\theta}{dt} = w + wi\frac{V'(\theta)}{V'^2(\theta) + w'^2(\theta)}, \tag{C.6}$$

where i is instantaneous scaled current from equation C.5 and $V'(\theta)$ is the only surviving element from $U_k^{'}$. Just as in our results, described below, this gives the phase resetting due to a perturbation by projecting the perturbation in voltage onto the limit cycle. However, the intuition behind this reasoning is described only in this article.

The most logical way to compare our results with those of Ermentrout and Kopell is to use the product form of the coupling $h_k(\theta_k, \theta_j) = P(\theta)R(\theta)$ and to set $P(\theta) = i$ and

$$R(\theta) = \frac{V'(\theta)}{V'^2(\theta) + w'^2(\theta)}. \tag{C.7}$$

This is not how Ermentrout and Kopell (1991a, b) defined $R(\theta)$ and $P(\theta)$: they included the presynaptic voltage terms in $R(\theta)$ and all postsynaptic terms in $P(\theta)$. Since they used a synaptic current for the perturbation rather than a square pulse, the current term $g_{ex}(V(\theta_j))(V_{ex} - V(\theta_k))$ was *not* equivalent to $R(\theta)$, and the $P(\theta)$ term included $(V_{ex} - V(\theta_k))$. On the other hand, we separated the terms into a term representing the dynamics near the original unperturbed limit cycle ($R(\theta)$) and a term representing the perturbation in voltage ($P(\theta)$). If you make the assumption that i is nonzero for a very brief period of time and that for simplicity the integral of i over this brief interval is 1 (like a delta function), then you can assume $R(\theta)$ is constant at its value at the time the perturbation is initiated. The θ on the left-hand side of equation C.6 varies with a constant angular velocity over most of the limit cycle (everywhere except when it receives a perturbation; see Figure 11). The temporal phase resetting in response to an instantaneous pulse is then a scaled version of $R(\theta)$ (see Figure 11):

$$F(\theta) = -w^{-1}R(\theta). \tag{C.8}$$

In our derivation, we define a new quantity σ, geometrical phase, that is distance along the limit cycle as a function of time. This function, unlike the temporal phase $\theta(t)$ used by Ermentrout and Kopell (1991a) and by Hoppensteadt and Izhikevich (1997) has a variable derivative along the limit cycle,

$$\sigma = s(t) = \frac{1}{L}\int_0^t ||\dot{u}(t)||dt, \tag{C.9}$$

where L is the length of the limit cycle in the appropriate coordinate system and the dot indicates the derivative with respect to time. Thus, $d\sigma = \| \dot{u}(t) \| dt$. We show that for Morris-Lecar,

$$d\sigma = \frac{\dot{V}(t)}{\sqrt{\dot{V}^2(t) + \dot{w}^2(t)}}. \tag{C.10}$$

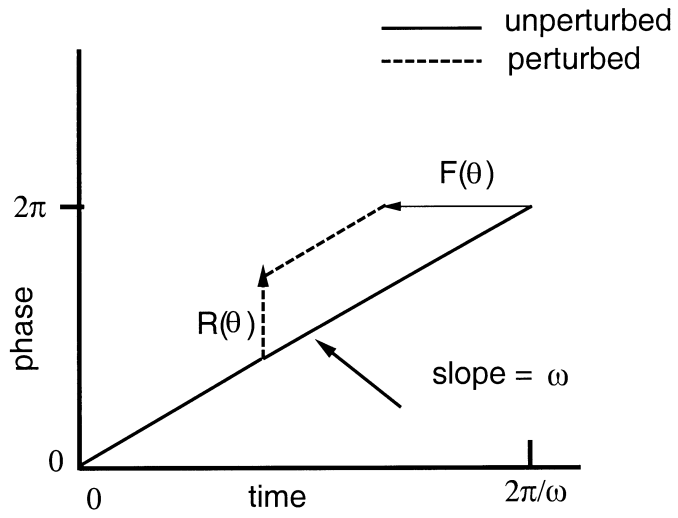

Figure 11: Relationship of PRC $F(\theta)$ to a change in angular displacement, $R(\theta)$. This is a plot of constant angular velocity of the temporal phase that indicates the resetting produced by Ermentrout and Kopell's (1991a, 1991b) $R(\theta)$.

From equation C.9, we see that for Morris-Lecar,

$$d\sigma = \sqrt{\dot{V}^2(t) + \dot{w}^2(t)}dt. \tag{C.11}$$

Furthermore, the temporal phase resetting (ϕ) can be obtained using the inverse of $s(t)$:

$$d\phi = s^{-1}(\sigma). \tag{C.12}$$

We can recover the result of Ermentrout and Kopell (1991a), for temporal phase resetting $R(\theta)$ given in equation C.8 by equating $R(\theta)$ with the instantaneous change in temporal phase dt due to a delta function perturbation and then substituting equation C.12 into C.11:

$$dt = \frac{V'(t)}{V'^2(t) + w'^2(t)}, \tag{C.13}$$

noting that in Ermentrout and Kopell, time t and phase ϕ are related by a constant.

The expression given in equation C.13 is the adjoint, or infinitesimal PRC, as given in equation 3.2 of Hansel, Mato, and Meunier (1995) and equation A21 of Ermentrout and Kopell (1991b), providing that variations in

amplitude (perturbations normal to the limit cycle) are ignored. Izhikevich (2000) also obtained a similar result, but in the limit as the derivative of the slow variable ($w'^2(t)$ in C.13) goes to zero. Although previous work in the literature contains expressions that are mathematically similar to the ones presented in this article, they do not contain the geometrical intuition presented here. This intuition allows for the possibility of extending PRC analysis to type II model neurons and even to physiological type II neurons for which we do not know the equations of state but for which we can reconstruct an attractor.

Acknowledgments

This work was supported by Whitaker Foundation grant TF-98-0033 and NSF grant IBN-0118117.

References

Abarbanel, H. D. I., Brown R., Sidorowich J. J., & Tsimring L. Sh. (1993). The analysis of observed chaotic data in physical systems. *Rev. Mod. Phys., 65*, (4), 1331–1392.

Abramovich-Sivan, S., & Akselrod, S. (1998a). A PRC based model of a pacemaker cell: Effect of vagal activity and investigation of the respiratory sinus arrhythmia. *J. Theor. Biol., 192*, 219–243.

Abramovich-Sivan, S., & Akselrod, S. (1998b). A phase response curve based model: effect of vagal and sympathetic stimulation and interaction on a pacemaker cell. *J. Theor. Biol., 192*, 567–579.

Arshavsky, Yu. I., Beloozerova, I. N., Orlovsky, G. N., Panchin, Yu, V., & Pavlova, G. A. (1985). Control of locomotion in marine mollusc Clione limacina I. Efferent activity during actual and fictitious swimming. *Exp. Brain Res., 58*, 255–262.

Baxter, R. J., Canavier, C. C., Lechner, H. A., Butera, R. J., DeFranceschi, A. A., Clark, J. W., & Byrne, J. H. (2000). Coexisting stable oscillatory states in single cell and multicellular neuronal oscillators. In D. Levine, V. Brown, and T. Shirley (Eds.), *Oscillations in neural systems* (pp. 51–77). Hillside, NJ: Erlbaum.

Beer, R. D., Chiel, H. J., & Gallagher, J. C. (1999). Evolution and analysis of model CPGs for walking II. General principles and individual variability. *J. Comp. Neurosci., 7*(2), 119–147.

Canavier, C. C., Baxter, D. A., Clark, J. W., & Byrne, J. H. (1999). Control of multistability in ring circuits of oscillators, *Biol. Cybernetics, 80*, 87–102.

Canavier, C. C., Butera, R. J., Dror, R. O., Baxter, D. A., Clark, J. W., & Byrne, J. H. (1997). Phase response characteristics of model neurons determine which patterns are expressed in a ring circuit model of gait generator. *Biol. Cybernetics, 77*, 367–380.

Chiel, H. J, Beer, R. D., & Gallager, J. C. (1999). Evaluation and analysis of model CPGs for walking: I dynamical models. *J. Comp. Neurosci., 7*, 1–20.

Collins, J. J., & Richmond, S. A. (1994). Hard-wired central pattern generators for quadrupedal locomotion. *Biol. Cyber., 71*, 375–385.
Collins, J. J., & Stewart, I. N. (1993). Coupled nonlinear oscillators and the symmetries of animal gaits. *J. Nonlin. Sci., 3*, 349–392.
Dror, R. O., Canavier, C. C., Butera, R. J., Clark, J. W., & Byrne, J. H. (1999). A mathematical criterion based on phase response curves for the stability of a ring network of oscillators. *Biol. Cybern., 80*, 11–23.
Ermentrout, G. B. (1985). The behavior of rings of coupled oscillators. *J. Math. Biol., 23*, 55–74.
Ermentrout, G. B. (1986). Parabolic bursting in an excitable system coupled with a slow oscillation. *SIAM J. Appl. Math., 46*, 233–253.
Ermentrout, G. B. (1994). *Neural modelling and neural networks*. Oxford: Pergamon Press.
Ermentrout, G. B. (1996). Type I membranes, phase resetting curves, and synchrony. *Neural Computation, 8*, 979–1001.
Ermentrout, G. B., & Kopell, N. (1991a). Oscillator death in systems of coupled neural oscillators. *SIAM J. Appl. Math., 29*, 195–217.
Ermentrout, G. B., & Kopell, N. (1991b). Multiple pulse interactions and averaging in coupled neural oscillators. *J. Math. Biol., 50*(1), 125–146.
FitzHugh, R. (1969). Mathematical models of excitation and propagation in nerve. In H. P. Schwan (Ed.), *Biological engineering* (pp. 1–10). New York: McGraw-Hill.
Foss, J., & Milton, J. (2000). Multistability in recurrent neural loops arising from delay. *J. Neurophysiology, 84*, 975–985.
Glass, L., & Mackey, M. (1988). *From clocks to chaos: The rhythms of life*. Princeton, NJ: Princeton University Press.
Golubitsky, M., Stewart, I., Buono, P. -L., & Collins, J. J. (1998). A modular network for legged locomotion. *Physica D, 115*, 56–72.
Guckenheimer, J., & Holmes, P. (1983). *Nonlinear oscillations, dynamical systems, and bifurcation of the vector fields*. Berlin: Springer-Verlag.
Hansel, D., Mato, G., & Meunier, C. (1995). Synchronization in excitatory neural networks. *Neural Computation, 7*, 307–337.
Hodgkin, A. L. (1948). The local electric changes associated with repetitive action in a non-medullated axon. *J. Physiology, 107*, 165–181.
Hoppensteadt, F. C., & Izhikevich, E. M. (1997). *Weakly connected neural networks*. New York: Springer-Verlag.
Izhikevich, E. M. (2000). Phase equations for relaxation oscillators. *SIAM J. Appl. Math., 60*, 1789–1804.
Kopell, N., & Ermentrout, G. B. (1988). Coupled oscillators and the design of central pattern generators. *Math. Biol., 90*, 87–109.
Mirollo, R. I., & Strogatz, S. H. (1990). Synchronization of pulse-coupled biological oscillators. *SIAM J. Appl. Math., 50*, 1645–1662.
Morris, C., & Lecar, H. (1981). Voltage oscillations in the barnacle giant muscle fiber. *Biophys. J., 35*, 193–213.
Murray, J. D. (1993). *Mathematical biology* (2nd ed.). New York: Springer-Verlag.
Nishii, J. (1999). Learning model for coupled neural oscillators. *Network: Comp. Neural Syst., 10*, 213–226.

Oprisan, S. A., & Canavier, C. C. (2000a). Phase response curve via multiple time scales analysis of the limit cycle behavior of type I and type II excitability. *Biophys. J., 78*, 218A.

Oprisan, S. A., & Canavier, C. C. (2000b). Analysis of central pattern generator circuits using phase resetting. *Soc. Neurosci. Abstr., 26*, 2000.

Oprisan, S. A., & Canavier, C. C. (2001). The structure of instantaneous phase resetting in a neural oscillator. *InterJournal of Complex Systems*, manuscript 386. Available on-line at: www.interjournal.org/.

Pavlidis, T. (1973). *Biological oscillators: Their mathematical analysis*. Orlando, FL: Academic Press.

Pinsker, H. M. (1977). Aplysia bursting neurons as endogenous oscillators: I: Phase-response curves for pulsed inhibitory synaptic input. *J. Neurophysiology, 40*, 527–543.

Rinzel, J., & Ermentrout, G. B. (1998). Analysis of neural excitability and oscillations. In C. Koch & I. Segev (Eds.), *Methods in neuronal modeling: From ions to networks* (pp. 251–292). Cambridge, MA: MIT Press.

Rinzel, J., & Lee, Y. S. (1986). On different mechanisms for membrane potential bursting. In H. G. Othmer (Ed.), *Nonlinear oscillations in biology and chemistry*. New York: Springer-Verlag.

Takens, F. (1981). Detecting strange attractors in turbulence. In D. A. Rand & L. S. Young (Eds.), *Proceedings of the Symposium on Dynamical Systems and Turbulence*. Berlin: University of Warwick.

Traub, R. D., & Miles, R. (1991). *Neural networks of the hippocampus*. Cambridge: Cambridge University Press.

Wilson, M. A., & Bower, J. M. (1989). The simulation of large scale neural networks. In *Methods in Neural Modeling*. Cambridge, MA: MIT Press.

Winfree, A. (1980). *The geometry of biological time*. New York: Springer-Verlag.

Received March 5, 2001; accepted July 25, 2001.